

PAPER • OPEN ACCESS

Phase estimation of local Hamiltonians on NISQ hardware

To cite this article: Laura Clinton *et al* 2023 *New J. Phys.* **25** 033027

View the [article online](#) for updates and enhancements.


You may also like

- [Observational entropy, coarse-grained states, and the Petz recovery map: information-theoretic properties and bounds](#)
Francesco Buscemi, Joseph Schindler and Dominik Šafránek
- [Phononic-subsurface flow stabilization by subwavelength locally resonant metamaterials](#)
Armin Kianfar and Mahmoud I Hussein
- [Correlation properties of a one-dimensional repulsive Bose gas at finite temperature](#)
Giulia De Rosi, Riccardo Rota, Grigori E Astrakharchik *et al.*



PAPER

Phase estimation of local Hamiltonians on NISQ hardware

Laura Clinton^{1,2,*} , Johannes Bausch^{1,3}, Joel Klassen¹ and Toby Cubitt¹¹ Phasecraft Ltd, London, United Kingdom² Department of Computer Science, University College London, London, United Kingdom³ CQIF, DAMTP, University of Cambridge, Cambridge, United Kingdom

* Author to whom any correspondence should be addressed.

E-mail: laura@phasecraft.io**Keywords:** quantum phase estimation, quantum computing, Hamiltonian simulation, pulse efficient compilation

OPEN ACCESS

RECEIVED
2 August 2022REVISED
27 February 2023ACCEPTED FOR PUBLICATION
8 March 2023PUBLISHED
27 March 2023Original Content from
this work may be used
under the terms of the
[Creative Commons
Attribution 4.0 licence](https://creativecommons.org/licenses/by/4.0/).Any further distribution
of this work must
maintain attribution to
the author(s) and the title
of the work, journal
citation and DOI.**Abstract**

In this work we investigate a binned version of quantum phase estimation (QPE) set out by Somma (2019 *New J. Phys.* **21** 123025) and known as the quantum eigenvalue estimation problem (QEEP). Specifically, we determine whether the circuit decomposition techniques we set out in previous work, Clinton *et al* (2021 *Nat. Commun.* **12** 1–10), can improve the performance of QEEP in the noisy intermediate scale quantum (NISQ) regime. To this end we adopt a physically motivated abstraction of NISQ device capabilities as in Clinton *et al* (2021 *Nat. Commun.* **12** 1–10). Within this framework, we find that our techniques reduce the threshold at which it becomes possible to perform the minimum two-bin instance of this algorithm by an order of magnitude. This is for the specific example of a two dimensional spin Fermi-Hubbard model. For example, we estimate that the depolarizing single qubit error rate required to implement a minimum two bin example of QEEP—with a 5×5 Fermi-Hubbard model and up to a precision of 10%—can be reduced from 10^{-7} to 10^{-5} . We explore possible modifications to this protocol and propose an application, which we dub randomized quantum eigenvalue estimation problem (rQEEP). rQEEP outputs estimates on the fraction of eigenvalues which lie within randomly chosen bins and upper bounds the total deviation of these estimates from the true values. One use case we envision for this algorithm is resolving density of states features of local Hamiltonians.

1. Introduction

One of the most important subroutines in quantum computing is the quantum phase estimation (QPE) algorithm. In 1994 Shor showed that a quantum computer can factor an integer in a number of steps polynomially increasing with the bit size of that integer—a task as yet not known to be possible on a classical computer [Sho97]. A little later, Kitaev [Kit95] came up with an alternative formulation of the factoring algorithm. A key subroutine in Kitaev's formulation of the factoring algorithm is QPE. QPE retrieves information about the eigenvalues of a unitary U by inducing a phase kickback—through repeated controlled applications of U —onto a readout register, to which a quantum Fourier transform (QFT) is then applied. In addition to the factoring algorithm, QPE appears as an essential subroutine in many other quantum algorithms; indeed it has been shown that QPE can be effectively applied to any problem efficiently solvable on a quantum computer [WZ06].

A task for which QPE is naturally suited is the retrieval of spectral information about local Hamiltonians, wherein U corresponds to time evolution under a given Hamiltonian and we are obtaining information about the energy eigenvalues of H . This spectral information may be readily applied to the study of natural physical systems, for example in characterizing the properties of materials [Kit04].

Given the clear value of QPE it is worth understanding to what extent the subroutine may be implemented on noisy intermediate scale quantum (NISQ) devices. In this context, minimizing both the number of qubits, and the circuit depth, are essential. Two features of QPE which contribute significantly to these costs are the application of a large coherent QFT, and the number of times a controlled unitary is applied. This motivates considering a modified form of QPE wherein the QFT is replaced with classical post

processing, and one attempts to retrieve as much spectral information as possible under a limited number of applications of the controlled unitary. This is the strategy employed recently in works by O'Brien *et al* [OTT19], Somma [Som19], and Lin and Tong [LT21] in investigating applications of QPE for NISQ devices. In this work we focus in particular on the quantum eigenvalue estimation problem (QEEP) proposed by Somma.

The limiting factor for the performance of these methods is the maximum time T for which one may perform the controlled unitary time evolution. In previous work [CBC21] it was proposed that one could leverage variable time two-qubit interactions at the hardware level to perform more efficient multi-qubit gate synthesis. Under a cost model wherein the duration of the hardware interaction is proportional to the time parameter of the two-qubit interaction, this method can yield significant improvements on the total wall-time cost of Hamiltonian simulation. Clearly such gains would have an impact on the performance of the phase estimation methods outlined above. In this paper we build on this work and consider the near-term feasibility of performing phase estimation on local Hamiltonians under this framework.

To do this we combine our gate synthesis techniques with QEEP. We find that our techniques significantly reduce the threshold at which it becomes possible to perform QEEP for a two dimensional spin Fermi-Hubbard model. For example, we estimate that the depolarizing single qubit error rate required to implement a minimum two bin example of QEEP—with a 5×5 Fermi-Hubbard model and up to a precision of 10%—can be reduced from 10^{-7} to 10^{-5} . We emphasize that this includes the benefits of both our synthesis techniques but also the modifications we suggest in appendix B, with each modification providing roughly an order of magnitude improvement. Furthermore, we reformulate QEEP as a general protocol to sample from a convolution between the spectrum of a Hamiltonian and a characterised class of functions. We then explore possible modifications to this protocol and propose an application, which we dub randomized quantum eigenvalue estimation problem (rQEEP), and explain how this may be used to estimate spectral properties such as density of states.

The outline of this paper is as follows. In section 2 we discuss some important preliminary details. These include: a review of our circuit error model, with a discussion of hardware and noise assumptions (section 2.1); a review of QPE with and without QFT (section 2.2); and a review of the QEEP (section 2.3). In section 3 we give a rigorous formulation of rQEEP, and show how this can be reduced to QEEP. In section 4 we discuss the details of applying sub-circuit methods to QEEP and perform a comprehensive numerical analysis of the expected run-time of QEEP using these methods. We illustrate how QEEP may be adapted to specific purposes by considering a modified version with a different smoothing function on the bins (section B.1). This modified version yields smaller bin sizes under a max time evolution T , when T is sufficiently small, but with a trade-off of worse asymptotic behaviour as T increases. Trade-offs of this type are particularly relevant in NISQ applications where minimising the circuit depth of the concrete problem instance is more important than optimal asymptotic scaling. The numerical analysis is performed for the time evolution on a spin-full Fermi-Hubbard model on a 3×3 and 5×5 grid (section 4.3). For each lattice size we analyse the performance with target precisions of 10%, 5% and 1%. We do not assume perfect hardware, but in the analysis we model the noise inherent to all NISQ hardware.

We find that our decomposition methods consistently reduce the threshold at which it becomes possible to perform a minimum working example of QEEP with two bins by an order of magnitude over the range of lattice sizes and target precisions considered. This suggests that one or two orders of magnitude improvement in quantum hardware are required before QEEP enters the scope of practical application on near term devices. In particular, the depolarizing noise rates we consider are extremely ambitious, and even with these noise rates we expect smaller bin widths are necessary for practically useful applications. In section 5 we consider various avenues for closing this gap.

2. Preliminaries

2.1. Circuit error model

Here we recap our theoretical abstraction of the hardware capabilities of NISQ-era devices [CBC21]. We describe three related concepts in this section: a circuit model, an error model, and a cost model. These concepts are summarized by definitions 1 and 2 and equation (1). The circuit model can describe any quantum computing architecture in which discrete gates are generated by continuous-time interactions between qubits, and where these interactions can effectively be described by a Hamiltonian—or effective Hamiltonian—coupling those qubits.

Many current matter-based quantum computing architectures fit this description, including superconducting circuits, most ion trap architectures and nuclear magnetic resonance (NMR) quantum computing (liquid-state or solid-state). Although this error model is a theoretical idealisation work has

recently been published which supports the validity of this model and demonstrates the advantages of exploiting analogue control [Ste+21].

We call this circuit model the subcircuit model and it is defined as follows.

Definition 1 (Sub-circuit model). Given a set of qubits Q , a set $I \subseteq Q \times Q$ specifying which pairs of qubits may interact, a fixed two qubit interaction Hamiltonian h , and a minimum switching time t_{\min} , a sub-circuit pulse-sequence C is a quantum circuit of L pairs of alternating layer types $C = \prod_l^L U_l V_l$ with $U_l = \prod_{i \in Q} u_i^l$ being a layer of arbitrary single qubit unitary gates, and $V_l = \prod_{ij \in \Gamma_l} v_{ij}(t_{ij}^l)$ being a layer of non-overlapping, variable time, two-qubit unitary gates:

$$v_{ij}(t) = e^{ith_{ij}}$$

with the set $\Gamma_l \subseteq I$ containing no overlapping pairs of qubits, and $t \geq t_{\min}$. Throughout this paper we assume $h_{ij} = Z_i Z_j$. As all $\sigma_i \sigma_j$ are equivalent to $Z_i Z_j$ up to single qubit rotations this can be left implicit and so we take $h_{ij} = \sigma_i \sigma_j$.

This defines the gate-set we have access to. We also refer to these gates as ‘sub-circuit’ as they exist one level of abstraction below the digital gate-set of the standard circuit model. We note that *any* standard quantum circuit can be expressed in this ‘sub-circuit’ form as up to single qubit rotations a controlled NOT or CNOT gate is equivalent to $e^{-i\frac{\pi}{4}ZZ}$. This means that we can cost standard circuits in our framework as sub-circuit gates with $t = O(1)$. We will use this fact in section 4.3. We will express all quantum circuits in terms of sub-circuit gates throughout this work. We do this so that we can cost all circuits under the same noise model.

The sub-circuit model is useful as it can distinguish circuits under an error model where errors accumulate proportionally to the time for which interactions are switched on. This is in contrast to traditional error models, where errors accumulate according to gate depth and all gates are costed equally. This leads us to the following error model. We will assume that errors accumulate proportionally to the time interactions in the system are switched on for. Formally, we assume that for Q qubits every layer l of sub-circuit gates in a circuit $C = \prod_l U_l V_l$ is interspersed with a single qubit depolarizing noise channel \mathcal{E} . For each qubit in layer l the channel is then approximated as

$$\mathcal{E}_l(\rho) : \rho \rightarrow (1 - q|t^l|)\rho + q|t^l|\frac{I}{2}, \quad (1)$$

for some noise parameter $q \in [0, 1]$ and where we have upper bounded each individual pulse-time in the l th-layer as $|t^l| := \max_{ij \in \Gamma_l} (|t_{ij}^l|)$.

Finally, we define the following cost model. We have assumed that errors accumulate based on the length of time two-qubit interactions are switched on for and therefore we cost circuits according to the following definition.

Definition 2 (Sub-circuit cost). The physical run-time of a sub-circuit pulse-sequence C is defined as

$$\mathcal{T}(C) := \sum_l^L \max_{ij \in \Gamma_l} (t_{ij}^l).$$

The run-time is normalised to the physical interaction strength, so that $|h| = 1$. This cost metric assumes that the single qubit layers contribute a negligible amount to the total time duration of the circuit.

This cost-metric will help us estimate what circuits can and cannot be implemented for a given depolarizing noise rate q if we are willing to tolerate a target error ϵ_{tar} .

This is captured by the following. We can calculate a trivial error bound by considering the probability that no error occurs at all. Let $\mathcal{U}(\rho)$ be the channel which implements circuit C without noise, and $\mathcal{U}'(\rho)$ the channel which implements circuit C with noise. Then for any measured observable O we get

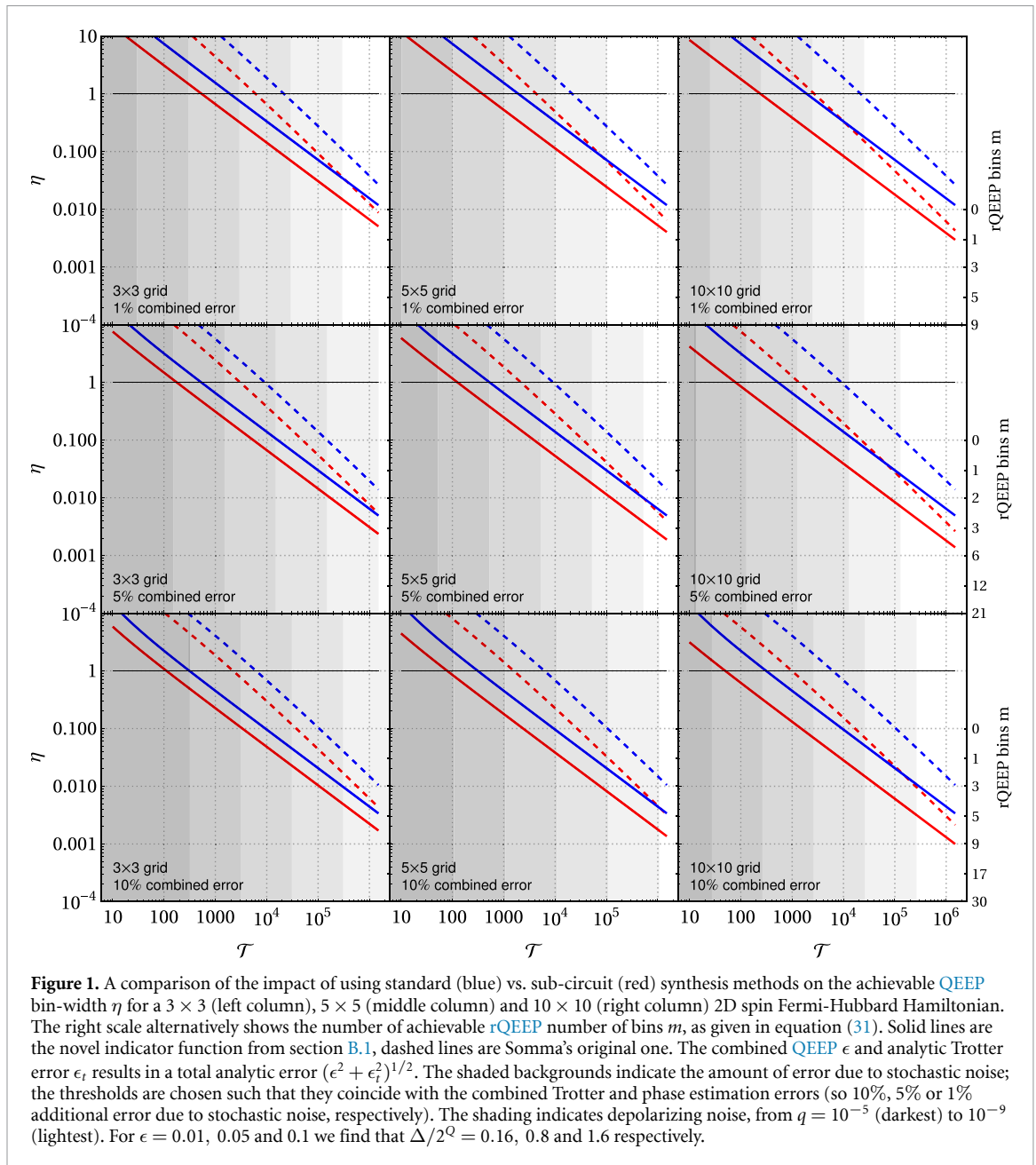
$$\epsilon := \text{Tr}[(\mathcal{U}(\rho) - \mathcal{U}'(\rho))O] \leq \epsilon_{\text{tar}}, \quad (2)$$

as we want to determine the maximum allowable run-time which keeps this stochastic error ϵ below a target error ϵ_{tar} .

This stochastic error ϵ is upper bounded by the probability that any error occurs in the circuit. For a Q -qubit circuit the noise channel defined above this gives us

$$\epsilon \leq 1 - \prod_l (1 - q|t^l|)^Q \quad (3)$$

$$\leq 1 - (1 - q)^V \leq \epsilon_{\text{tar}}, \quad (4)$$



where $V = Q \times \mathcal{T}(C)$ is the volume of the circuit and $\mathcal{T}(C) = \sum_l |t^l|$. Inverting this, we say that given an error parameter $q \in [0, 1]$, we can only implement circuits whose run-time is bounded as

$$\mathcal{T}(C) \leq \frac{\log(1 - \epsilon_{\text{tar}})}{Q \log(1 - q)}, \quad (5)$$

assuming we are willing to tolerate a stochastic error rate at most ϵ_{tar} . We will use this in section 4.3 and particularly in figure 1. These are the key assumptions we make in our circuit error model. In summary, we assume there is sufficient analogue control to express circuits in the sub-circuit form of definition 1 and that depolarizing noise in the device can be described by equation (1). This in turn makes the cost-metric of definition 2 useful as then the trivial stochastic error bound equation (5) can help us estimate requisite depolarizing error rates q for a given task. Our analysis and benchmarking in section 4 will follow this logic.

Having established this circuit error model in our previous work [CBC21], we also derived novel exact gate synthesis techniques to minimize the sub-circuit cost \mathcal{T} in this error model. These results can be summarized as follows. For a k -local Pauli interaction P_k , there exists a sub-circuit pulse-sequence $C := \prod_l^L U_l V_l$ which implements the evolution operator e^{-itP_k} . Most importantly, for any target time t the run-time of that circuit is bounded as

$$\mathcal{T}(C) \leq O\left(|t|^{\frac{1}{k-1}}\right), \quad (6)$$

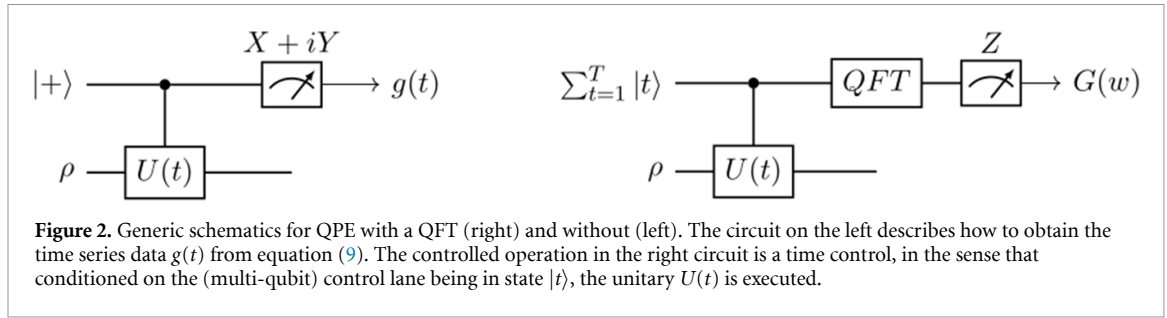


Figure 2. Generic schematics for QPE with a QFT (right) and without (left). The circuit on the left describes how to obtain the time series data $g(t)$ from equation (9). The controlled operation in the right circuit is a time control, in the sense that conditioned on the (multi-qubit) control lane being in state $|t\rangle$, the unitary $U(t)$ is executed.

according to the notion of run-time established in definition 2. Note that this is the scaling in terms of $|t|$, with k assumed to be a constant. We see from this that we can only expect an advantage for smaller values of k . The details of the decompositions which accomplish this can be found in our previous work [CBC21, appendix B]. Here we only note that they are exact and minimize $\mathcal{T}(C)$ as $t \rightarrow 0$ at the expense of increased circuit depth.

2.2. QPE by classical post processing

Let $f(t)$ be an integrable function. For consistency with past literature we adopt the convention for the Fourier transform and its inverse to be

$$F(w) = \mathcal{F}[f](w) = \frac{1}{2\pi} \int_{\mathbb{R}} f(t)e^{-iwt} dt, \quad \text{and} \quad \mathcal{F}^{-1}[F](t) = \int_{\mathbb{R}} F(w)e^{iwt} dw. \quad (7)$$

For a periodic function f one can express $f(t)$ as a Fourier series via

$$f(t) = \sum_{w=-\infty}^{\infty} F_w e^{iwt} \quad \text{with coefficients} \quad F_w := F(w). \quad (8)$$

With these conventions, the Fourier inversion theorem reads $\mathcal{F}^{-1} = \mathcal{FR}$ for the reflection functional $R[f](t) := f(-t)$.

QPE describes a family of quantum algorithms for retrieving information about the phases ϕ_j associated with the eigenvalues $e^{i\phi_j}$ of a unitary operator U . Such a unitary operator is generated by a Hermitian operator H via $U = \exp(-iH) = \sum_n \exp(-i\lambda_n) |\phi_n\rangle\langle\phi_n|$, where $\{\lambda_n\}$ are the eigenvalues of H —which are equivalent to the phases ϕ_j of U modulo 2π —and where the $\{|\phi_n\rangle\}$ are the (same) eigenvectors of H and U , respectively.

All variants of phase estimation may be thought of in the following terms. Consider some input state ρ and a time evolution operator $U(t)$ with phases $\{\phi_j\}$ and eigenstates $\{|\phi_j\rangle\}$. Prepare some time series data

$$g(t) := \sum_n e^{i\phi_n t} \langle\phi_n|\rho|\phi_n\rangle, \quad (9)$$

and extract information about the spectrum of this data

$$G(w) := \mathcal{F}[g] = \sum_i \delta(w - \phi_i) \langle\phi_i|\rho|\phi_i\rangle. \quad (10)$$

In the original phase estimation protocol—illustrated in figure 2—this process is performed coherently. First one prepares the desired input state $\rho = \rho_I$ on an input register I , and a coherent superposition of time states $\sum_{t=1}^T |t\rangle$ on a control register C . The time register then controls the unitary time evolution on register I , to obtain

$$\rho_{CI} \propto \sum_{tt'} |t\rangle\langle t'|_C \otimes U(t)\rho_I U(t')^\dagger. \quad (11)$$

Tracing out the input register then yields time series data, namely

$$\text{Tr}_I(\rho_{CI}) =: \rho_C \propto \sum_n \sum_{tt'} |t\rangle\langle t'|_C e^{-i\phi_n t} \langle\phi_n|\rho_I|\phi_n\rangle e^{i\phi_n t'} = \sum_{tt'} g(t' - t) |t\rangle\langle t'|_C. \quad (12)$$

The QFT is applied, and we obtain

$$\text{QFT}(\rho_C) \propto \sum_{ww'} \left(\sum_{tt'} e^{-iwt+iw't'} g(t'-t) \right) |w\rangle\langle w'|_C. \quad (13)$$

Measuring the control qubits in the computational basis is equivalent to sampling from $G(w)$ over possible n -bit values of w .

Applying QPE to problems involving local Hamiltonians differs significantly from its application to factoring in two important ways. First, it is unlikely that one can construct a polynomial depth circuit decomposition of $U(T)$ for exponentially large T [AA17].

Second, the size of a problem involving a local Hamiltonian goes as the number of qubits. As the number of qubits grows, the number of eigenvalues increase exponentially, but the spectral range of the Hamiltonian increases polynomially⁴. It is the spectral range of the Hamiltonian which determines the bandwidth of $g(t)$, and so it is not clear that the inclusion of a QFT should yield significant gains for such problems. If on the other hand one wishes to resolve fine-grained details of $G(w)$, then from a classical signal processing perspective the parameter which dictates this resolution is the maximum simulated time T , not the number of samples of $g(t)$.

This motivates an alternative method, which avoids the use of an expensive QFT. Instead of preparing and processing a coherent superposition of $g(t)$ sampled at an exponential number of time steps, $g(t)$ is directly measured for a polynomial number of time steps up to a maximum time T , and this data is processed classically. The procedure for measuring $g(t)$ (illustrated in figure 2) is a straightforward phase kickback protocol, where the control register is prepared in the $|+\rangle$ state, the input register is prepared with the input state ρ_I , and a controlled time evolution is applied

$$\rho_{CI} = \frac{1}{2} \sum_{ij=0}^1 |i\rangle\langle j| \otimes U(t)^i \rho_I U(-t)^j. \quad (14)$$

Measuring the expectation value of $X + iY$ on the control register yields:

$$\langle X_C \rangle + i \langle Y_C \rangle = \text{Tr}[\rho_I U(t)] = \sum_i e^{-i\phi_i t} \langle \phi_i | \rho_I | \phi_i \rangle = g^*(t) = g(-t). \quad (15)$$

Equipped with a quantum black box for values of $g(t)$ it would appear that the remainder of the problem is merely a classical signal processing problem, about which a rich body of literature exists. However the existing classical signal processing literature typically assumes that the signal is composed of a polynomial number of frequencies, which is not generally true for a signal as in equation (9) composed of up to exponentially many distinct eigenvalues of the Hamiltonian of interest.

2.3. The QEEP algorithm

As outlined in the last section, resolving all exponentially many eigenvalues of a Hamiltonian is costly, as it would require us to simulate an exponential time evolution under H . Yet it is conceivable that one can obtain approximate information about the spectrum in a more efficient manner. Such an algorithm was introduced by [Som19] and we recap it here. The QEEP—as defined by [Som19]—is just such an approximation. In contrast to the ambitious goal of obtaining exponentially many eigenvalues for an operator H , the range of possible eigenvalues is divided up into bins, and the aim is to estimate the fraction of eigenvalues in each bin up to some smoothing on the boundaries of the bin.

Quantum eigenvalue estimation problem (QEEP)

Input:	A Hamiltonian H with associated eigenvalues $\{\lambda_i\}$ and eigenvectors $\{ \lambda_i\rangle\}$. An input quantum state ρ . A bin width $\eta > 0$, precision parameter $\epsilon > 0$ and confidence level $c < 1^5$. An indicator function $f(w) : \mathbb{R} \rightarrow [0, 1]$ s.t. $\forall w \notin [-\eta, \eta] : f(w) = 0$ and $\forall w \in [0, \eta] : f(w) + f(w - \eta) = 1$.
Promise:	$\ H\ _\infty \leq 1/2$.
Question:	A vector $\mathbf{q} = (q_0, q_1, \dots, q_M)$ with $M = \lfloor 1/\eta \rfloor$ s.t. with probability $\geq c$, $\ \mathbf{q} - \mathbf{p}\ _1 \leq \epsilon$. Here $p_j = p(w_j) := \sum_i f(\lambda_i - w_j) \langle \lambda_i \rho \lambda_i \rangle$, and $w_j = j\eta - 1/2$.

⁴ The spectral norm is upper bounded by the sum of the norm of the local terms.

⁵ In Somma's original construction the bin width η is equal to the precision parameter ϵ . We have decoupled them, since they are conceptually distinct.

More specifically if one sets the input state to be the maximally mixed state this becomes $p_j = p(w_j) := \sum_i f(\lambda_i - w_j) 2^{-Q}$, where Q is the number of qubits.

The indicator function f in QEEP may be thought of as delineating the ‘shape’ of a bin. The values p_j can be thought of as the probability of observing the initial state ρ within a certain energy band, centred around $j\eta - 1/2$, whose resolution and sharpness is determined by the indicator function f . Equivalently, one may understand the values p_j as evenly spaced samples of $G(w)$ convolved with f :

$$p(w) = [G * f](w). \quad (16)$$

Depending on the choice of f , solutions to a QEEP instance might have varying applications, and may be easier or harder to solve. A general scheme for constructing a function f satisfying the conditions outlined in the problem statement is to take the ideal indicator function

$$\text{rect}_\eta(w) = \begin{cases} 1 & w \in [-\eta/2, \eta/2] \\ 0 & \text{otherwise} \end{cases} \quad (17)$$

and convolve it with a normalized smoothing kernel $h(w) \in [0, 1]$ with support only in $[-\eta/2, \eta/2]$ ⁶ to obtain

$$f(w) = [\text{rect}_\eta * h](w). \quad (18)$$

The algorithm that Somma proposes for resolving QEEP relies on the following signal processing principle. For a well chosen smoothing kernel h , the Fourier transform $P(t) := \mathcal{F}[p](t)$ of $p(w)$ may be made to fall off rapidly beyond a maximum time T , by smoothing out the sharply varying spectral function $G(w)$. Furthermore, since $p(w)$ has bounded support, $P(t)$ need only be sampled at a finite rate. Thus, one need only sample $g(t)$ at a finite rate to a maximum time T to retrieve a good approximation to the values p_j .

More precisely, we may consider that since $G(w)$ and $f(w)$ have bounded support they may be taken to be 2π periodic⁷ and decomposed into Fourier series expansions:

$$G(w) = \frac{1}{2\pi} \sum_{t=-\infty}^{\infty} g_{-t} e^{itw} \quad \text{with} \quad g_t = g(t) \quad (19)$$

$$f(w) = \sum_{t=-\infty}^{\infty} F_t e^{itw} \quad \text{with} \quad F_t = \mathcal{F}[f](t) \quad (20)$$

and thus:

$$p(w) = [G * f](w) = \int_{-\infty}^{\infty} G(w') f(w - w') dw' = \sum_{t=-\infty}^{\infty} e^{itw} F_t g_{-t}. \quad (21)$$

For fixed values $w_j = -1/2 + j\eta$ we retrieve

$$p_j = \sum_{t=-\infty}^{\infty} F_t^j g_{-t}, \quad F_t^j = e^{itw_j} F_t. \quad (22)$$

In Somma’s construction the indicator function $f(w)$ is defined as in equation (18), with a smoothing kernel $h(w) = a \exp(-1/(1 - (cw)^2))$. With appropriate scaling (correct choice of c and normalization $a \approx 2.25$). It is then argued that for any bin width η there exists some constant $\alpha > 1$ such that for all $|t| \geq \alpha/\eta$

$$|F_t| \leq \eta \exp\left(-\sqrt{|t|\eta/2}\right). \quad (23)$$

⁶ Demanding that $h(w)$ is normalized as $\int h(\omega) d\omega = 1$ ensures that $\forall w \in [0, \eta] : f(w) + f(w - \eta) = 1$.

⁷ Note that the period could be chosen tighter than 2π as $G(w)$ is bounded within $[-1/2, 1/2]$, which will likely yield a small constant improvement in the overall cost. We will not analyse this here.

Thus truncating the sum in equation (22) up to some maximum value $T \geq \alpha/\eta$ yields an approximation

$$p'_j = \sum_{t=-T}^T F_t^j g_{-t} \quad (24)$$

such that $\|\mathbf{p}' - \mathbf{p}\| \leq \frac{\epsilon}{2}$. We include an explicit computation of this maximum value T in appendix B. However we emphasize that this is an asymptotic result, and that finding α is a non-trivial task. For this reason we also consider a different indicator function in section B.1.

In addition to the source of error from this truncation, there is a source of error stemming from imperfect measurements of $g(t)$. It is assumed that the T -dimensional vector of actual measurements $\tilde{\mathbf{g}}$ satisfies $\|\tilde{\mathbf{g}} - \mathbf{g}\|_1 \leq \epsilon/2$ with probability greater than the confidence parameter c . Thus one retrieves a vector \mathbf{q} given by

$$q_j = \sum_{t=-T}^T F_t^j \tilde{g}_{-t} \quad (25)$$

such that $\|\mathbf{q} - \mathbf{p}\|_1 \leq \epsilon$ with probability greater than c . Further details concerning this can be found in [Som19]. Importantly c depends on the number of repetitions of the circuit depicted in figure 2; and not the maximum evolution time T .

Choosing the 1-norm yields bounds on the *overall* deviation from the ideal vector \mathbf{p} . One may consider other norms, such as the max norm, which bounds the *maximum* deviation, and yields a milder variant of Somma's error bound. For completeness and for the purpose of deriving explicit constants in the error bounds we walk through Somma's error derivation in detail in appendix B.

3. Randomized QEEP

3.1. Problem definition

As discussed in the introduction, a fundamental numerical primitive is to ask for eigenvalues for a given normal or Hermitian operator A . More specifically, given a Hermitian matrix A , the task is to return its spectrum—the set of its eigenvalues—up to some bit precision b , i.e. numerical accuracy $\xi = 2^{-b}$. Instead of speaking of the numeric precision with which results are obtained, one can take the viewpoint that such a function sorts A 's eigenvalues into 2^b many bins of width $\propto \xi$. Such a function is e.g. implemented in matlab's `eig` or Mathematica's `Eigenvalues` functions. Assuming no other numerical errors are present during the calculation⁸, we expect the result to be such that eigenvalues are rounded to their nearest bin.

As currently formulated, the QEEP contains overlapping indicator functions $f^j(\omega) := f(\omega - \omega_j)$, so that an eigenvalue in the support of both f^j and f^{j+1} will contribute to both p_j and p_{j+1} . There is an important reason for formulating QEEP in this manner. Consider what a 'perfect' choice of non-overlapping $f^j(\omega)$ might look like. As described in [Som19], the natural choice would be an indicator function such as

$$f(\omega) = \begin{cases} 1 & -\eta/2 \leq \omega < +\eta/2 \\ 0 & \text{otherwise.} \end{cases} \quad (26)$$

This choice would resolve the spectrum perfectly; and furthermore remove $f(\omega)$ from the input of the problem statement. However, as explained by the author of [Som19] the slow decay of the Fourier coefficients would mean one would have to simulate e^{-iTH} for impractically large T . Due to this one must choose a smooth $f(\omega)$ which approximates this ideal solution through having smoothly decaying support over $-\eta \leq \omega < +\eta$. That is to say the indicator functions overlap each other so that $\forall w \in [0, \eta] : f(w) + f(w - \eta) = 1$.

To address these considerations we formulate a problem which we call the rQEEP for short, which is close in spirit to Matlab's `eig` or Mathematica's `Eigenvalues` function. For a given H rQEEP outputs a binned estimate of the spectrum up to a probabilistic guarantee on the likelihood that eigenvalues close to bin boundaries have been misplaced; and which replaces the issue overlapping bins with *randomly defined* bins. We will now define this problem formally and then propose an algorithm to solve rQEEP via a reduction to QEEP.

⁸ Arbitrary precision arithmetic or internal arithmetic can give certain guarantees on the precision of the eigenvalues obtained.

Randomized quantum eigenvalue estimation problem (rQEEP)

Input:	Local Hamiltonian $H = \sum_i h_i$. Maximal point spacing $\xi > 0$, deviation $\Delta \geq 0$, and confidence $c \in [0, 1]$.
Promise:	$\text{spec}(H) \subseteq [-1/2, 1/2]$.
Output:	$m := 2/\xi$. List of coordinates (x_i, y_i) for $i = 1, \dots, (m+1)$ with $x_0 := -1/2$ and $x_{m+1} := 1/2$, such that <ul style="list-style-type: none"> 1. x_i are randomly but uniformly spaced, i.e. for all $x \in [-1/2, 1/2]$ there exists a x_i s.t. $x - x_i < \xi/4$, and the distance between neighbouring points is bounded by $x_i - x_{i-1} < \xi$. 2. The total absolute difference between the estimated (y_i) and true (n_i) number of eigenvalues of H within the interval $B_i = [x_{i-1}, x_i]$ is upper bounded—with probability greater than c—by the deviation Δ, i.e. $\sum_i y_i - n_i \leq \Delta$.

We first remark that the above problem is well-defined: indeed, we can always first obtain the entire spectrum of H to sufficient precision, and choose the abscissas such that the intervals B_i never have an eigenvalue on their boundaries (which is possible even with the restriction of $n = \text{poly}1/\xi$, as the spectrum of H is finite); and then define y_i as the number of eigenvalues within that interval. This answers the problem even for deviation $\Delta = 0$ and confidence $c = 1$.

Naturally, what we will be interested in is whether we can answer rQEEP efficiently, and for which sets of parameters we can do so.

3.2. Reducing rQEEP to QEEP

Given a local Hamiltonian $H = \sum_i h_i$ acting on Q qubits (which we assume to be rescaled such that the spectrum lies within $[-1/2, 1/2]$), we can solve the rQEEP by using QEEP as a subroutine and given access to a QEEP solver with a sub-circuit cost of $\mathcal{T}(Q, \eta, \epsilon, c)$. We do this via the following algorithm.

- (a) Given a maximal point spacing $\xi > 0$, deviation $\Delta \geq 0$, and confidence $c \in [0, 1]$ uniformly partition the interval $[-1/2, 1/2]$ into $m := 2/\xi$ many segments

$$\left[-\frac{1}{2}, -\frac{1}{2} + \frac{\xi}{2}\right) \cup \left[-\frac{1}{2} + \frac{\xi}{2}, -\frac{1}{2} + \xi\right) \cup \dots \cup \left[\frac{1}{2} - \frac{\xi}{2}, \frac{1}{2}\right] =: S_1 \cup \dots \cup S_m. \quad (27)$$

- (b) With confidence c run the following subroutine $\lceil \log_{(1-\frac{\xi}{2})}(1-c) \rceil$ times, and collect the results in a list:
1. Within each segment, choose x_i uniformly at random from S_i . Set $x_0 := -1/2$, and $x_{m+1} := 1/2$.
 2. Solve a QEEP instance with a suitable indicator function f , input state $\rho = I/2^Q$, bin width $\eta := \Delta/(6 \times 2^{Q+1}(m+1)^2)$, precision $\epsilon = \Delta/(8 \times 2^{Q+1})$, and confidence c . Denote the output with $q = (q_0, \dots, q_M)$ where $M = \lfloor 1/\eta \rfloor$, for the bins centred around $w_j = -1/2 + j\eta$ for $j = 0, \dots, M$.
 3. For all $i = 0, \dots, m$, define lower and upper envelopes via

$$y_i^{\text{lower}} := 2^Q \sum_{w_j \in R_i^{\text{lower}}} q_j \quad \text{and} \quad y_i^{\text{upper}} := 2^Q \sum_{w_j \in R_i^{\text{upper}}} q_j \quad (28)$$

$$R_i^{\text{lower}} := [x_i + \eta, x_{i+1} - \eta] \quad \text{and} \quad R_i^{\text{upper}} := [x_i - \eta, x_{i+1} + \eta] \quad (29)$$

and where we implicitly assume $R_i^{\text{lower}} = \emptyset$ if $x_i + \eta > x_{i+1} - \eta$.

4. Return $y_i := (y_i^{\text{lower}} + y_i^{\text{upper}})/2$.

- (c) Return the result from the subloop with the smallest deviation of lower and upper bounds.

This is illustrated in figure 3. In appendix A we prove the above algorithm has the following quantum overhead

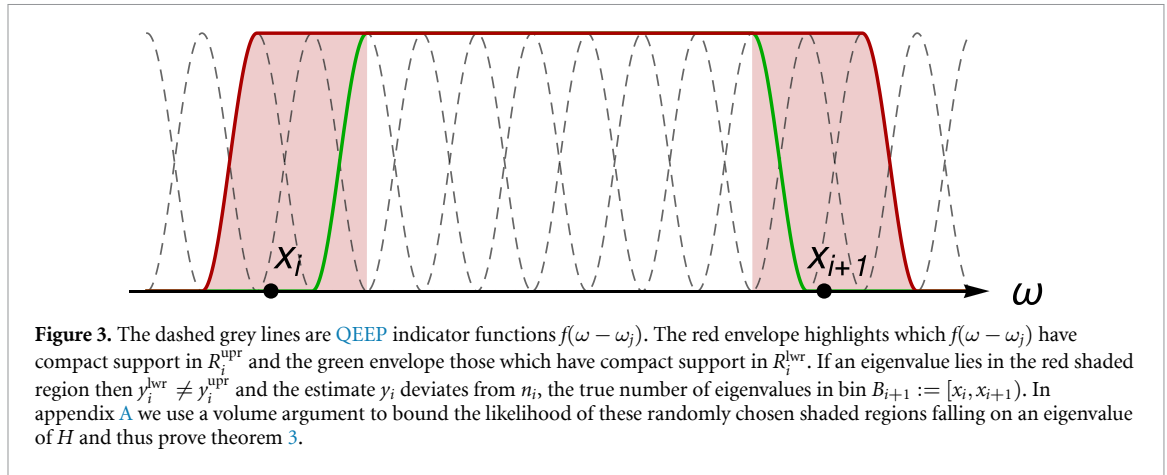
Theorem 3. *Given access to a QEEP solver with a subcircuit runtime $\mathcal{T}(Q, \eta, \epsilon, c)$ then the following holds. For a point spacing $\xi > 0$ (or equivalently $m := 2/\xi$), deviation $\Delta \geq 0$, and confidence c , the overall subcircuit runtime to answer rQEEP using QEEP is*

$$\mathcal{T}\left(Q, \frac{1}{12(m+1)^2} \times \frac{\Delta}{2^Q}, \frac{1}{16} \times \frac{\Delta}{2^Q}, c\right), \quad (30)$$

and the additional classical overhead is $\log_{(1-\frac{\xi}{2})}(1-c)$.

Using theorem 3 we can solve for m and Δ in terms of ϵ , η and Q and find the following dependence

$$m = \sqrt{\frac{4\epsilon}{3\eta}} - 1 \quad (31)$$



$$\Delta = 2^Q \times 16\epsilon. \quad (32)$$

Equations (31) and (32) tells us the number of bins and deviation with which we can expect when solving an instance of rQEEP given access to a QEEP solver which can achieve a bin width of η and a precision ϵ . The question is whether this now allows us to solve a problem of interest. The total deviation Δ refers to maximum number of misplaced eigenvalues. From the above we see that the total fraction of misplaced eigenvalues is proportional to ϵ , even though the total number scales as 2^Q .

The runtime \mathcal{T} depends on this η and ϵ . If we assume that we can solve QEEP efficiently for $\eta, \epsilon = \text{poly}(Q^{-1})$, then we can expect to efficiently solve rQEEP for a polynomially scaling number of bins $m = \text{poly}(Q)$ and a polynomially scaling fraction of misplaced eigenvalues, $\Delta/2^Q = \text{poly}(Q^{-1})$.

From [HMH04, HMH05] we know that for typical Hamiltonians the energy distribution will become Gaussian as $Q \rightarrow \infty$. Therefore we do not expect to be able to resolve features in the low energy subspace in this limit. Additionally, from [BFS11] we know that the computational difficulty of calculating the density of states for local Hamiltonians is in the counting version of QMA (known as #BQP) and so we cannot use rQEEP to do this efficiently.

However, we could still determine important features of the spectrum. The existence of a Mott insulator transition in Fermi-Hubbard models, and the Hamiltonian parameters for which this transition occurs, are of widespread interest [IFT98]. As the Mott insulator phase features a spectral gap we could try to observe this with rQEEP for a fixed number of qubits Q but while varying parameters such as the strength of on-site and hopping interactions.

4. Implementing and benchmarking QEEP and rQEEP for Fermi-Hubbard

4.1. Sub-circuit implementation with local controls

In this section we propose an alternative protocol to obtain g_t using several geometrically local control ancillas in place of a single globally connected ancilla as described in [Som19].

We consider a reasonably general case. Suppose we wish to solve QEEP for a k -local qubit Hamiltonian, $H = \sum_i \alpha_i h_i$. As we are interested in the NISQ era algorithms we will assume that when laid out on hardware, every Pauli interaction h_i acts non-trivially on geometrically local qubits. Furthermore we assume that the device has sufficient connectivity so that we can introduce a geometrically local ancilla qubit for each of these interactions. We denote these ancillas by dashed indices, i' , in contrast to the data qubits with undashed indices. This is illustrated for a two-local Hamiltonian with two terms in figure 4.

Over the joint Hilbert space we define an augmented Hamiltonian

$$H' := \sum_{i=1} \alpha_i Z_{i'} \otimes h_i. \quad (33)$$

To obtain time series data g_t from this augmented Hamiltonian, we first prepare a cat state on the control ancillary space, C . For $\rho_I = |\psi\rangle\langle\psi|_I$ the overall input is

$$|\psi(0)\rangle_{CI} = \frac{1}{\sqrt{2}}(|00\dots 0\rangle_C + |11\dots 1\rangle_C) \otimes |\psi\rangle_I. \quad (34)$$

On this initial state, the cat state induces a sign flip on the augmented Hamiltonian H' , conditioned on the cat state to be in state $|1\rangle_C$; more precisely, applying the evolution operator $U'_c(t) := \exp(itH'/2)$ we get

$$|\psi(t)\rangle_{CI} = \frac{1}{\sqrt{2}} \left(|00\dots 0\rangle_C e^{itH/2} |\psi\rangle_I + |11\dots 1\rangle_C e^{-itH/2} |\psi\rangle_I \right), \quad (35)$$

as can be readily verified. By measuring the expectation value $g_t = \langle X_{1'} + iY_{1'} \rangle_{\rho(t)}$ for $\rho(t) = |\psi(t)\rangle\langle\psi(t)|_{CI}$ we obtain the time series data g_t , as desired.

4.2. Asymptotic run-time analysis

In this section we will establish the run-time of the single most costly experiment involved in solving QEEP for $H = \sum_i \alpha_i h_i$. That is we will calculate the run-time—specified by definition 2—associated with the protocol to obtain g_T outlined in section 4.1.

In previous work [CBC21] we establish tighter bounds on the run-time of implementing $U(T) = e^{-iTH}$ where $H = \sum_i \alpha_i h_i$ is a k -local Hamiltonian with $\alpha_i \leq 1$ and $\|h_i\| = 1$. First we decompose $U(T)$ via a Trotter approximation, that is set $U(T) \approx (\prod_i e^{i\delta\alpha_i h_i})^{T/\delta} + O(T\delta)$, and then use the sub-circuit synthesis techniques given in [CBC21] to implement each local Trotter step $e^{i\delta\alpha_i h_i}$ with sub-circuit run-time $\mathcal{T}(e^{i\delta\alpha_i h_i}) \approx O(\delta^{1/(k-1)})^9$.

In order to perform QEEP with local control as described in the previous section we must instead implement $U'_c(T) = e^{-iTH'}$ where $H' = \sum_i \alpha_i Z_{i'} h_i$ in the manner described above. Now the run-time of each local Trotter step is $\mathcal{T}(e^{i\delta\alpha_i Z_{i'} h_i}) \approx O(\delta^{1/k})$. As there are T/δ Trotter steps this means

$$\mathcal{T}(U'_c(T)) \leq O\left(T\delta^{-\frac{1}{k}}\right). \quad (36)$$

This diverges as $\delta \rightarrow 0$. Therefore, we must choose the largest δ for a given Trotter error ϵ^{10} . That is we choose the value of δ which saturates the inequality $\epsilon \geq O(T\delta)$. Substituting this into equation (36) gives

$$\mathcal{T}(U'_c(T)) \leq O\left(T^{1+\frac{k-1}{k}} \epsilon^{-\frac{k-1}{k}}\right). \quad (37)$$

As discussed in section B.1, T will depend in the bin-width η and precision. We will use the bound equation (69) to determine this, meaning

$$\mathcal{T}(U'_c(T)) \leq O\left(T^{1+\frac{k-1}{k}} \epsilon^{-\frac{k-1}{k}}\right) \quad \text{with} \quad T \rightarrow \frac{\pi}{\eta} \times \frac{e^{\pi\eta\epsilon/2}}{\sqrt{e^{\pi\eta\epsilon} - 1}}. \quad (38)$$

This run-time does not take any connectivity assumptions into account, however we will address the issue of connectivity in our numeric benchmarking of this approach in section 4.3. As we are interested in the NISQ regime we will focus on a numerical analysis of a specific example Hamiltonian, the 2D spin Fermi-Hubbard Hamiltonian, rather than an asymptotic analysis of the general algorithm.

4.3. Numerical results for the Fermi-Hubbard model

We will take the following problem instance; a rQEEP input Hamiltonian which is a two-dimensional $L \times L$ lattice Fermi-Hubbard model with spin. This Hamiltonian is made up of on-site interactions and nearest neighbour hopping terms

$$H := \sum_{i=1}^{L^2} h_{\text{on-site}}^{(i)} + \sum_{i<j,\sigma} h_{\text{hopping}}^{(i,j,\sigma)} \quad (39)$$

$$:= u \sum_{i=1}^{L^2} a_{i\uparrow}^\dagger a_{i\uparrow} a_{i\downarrow}^\dagger a_{i\downarrow} + v \sum_{i<j,\sigma} \left(a_{i\sigma}^\dagger a_{j\sigma} + a_{j\sigma}^\dagger a_{i\sigma} \right) \quad (40)$$

which describe electrons; and with spin $\sigma = \uparrow$ or \downarrow hopping between neighbouring sites on a lattice, with an on-site interaction between opposite-spin electrons at the same site. We will assume that this fermionic Hamiltonian has been encoded into a qubit Hamiltonian using the compact fermion encoding [Der+21]. This first requires us to decide on the layout of qubits, as shown in figure 5. This figure shows the layout of a single spin sector for $L = 3$ on a device with planar connectivity. First the on-site interaction becomes,

⁹ This is an abuse of notation as there are many circuits which implement a given U . Therefore $\mathcal{T}(U)$ is not well defined, however if it is clear from context what circuit we are using to decompose U we write $\mathcal{T}(U)$ for readability.

¹⁰ Here we take the Trotter error to be the same as the precision to which we implement QEEP.

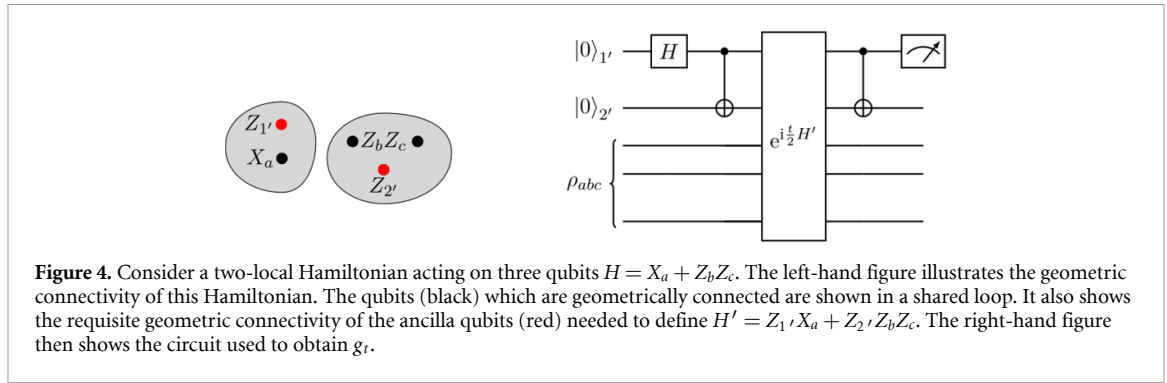


Figure 4. Consider a two-local Hamiltonian acting on three qubits $H = X_a + Z_b Z_c$. The left-hand figure illustrates the geometric connectivity of this Hamiltonian. The qubits (black) which are geometrically connected are shown in a shared loop. It also shows the requisite geometric connectivity of the ancilla qubits (red) needed to define $H' = Z_1 X_a + Z_2 Z_b Z_c$. The right-hand figure then shows the circuit used to obtain g .

$$h_{\text{on-site}}^{(i)} \rightarrow \frac{u}{4} (I - Z_{i\uparrow}) (I - Z_{i\downarrow}). \quad (41)$$

The exact expressions for hopping interactions are more complicated and depend on whether two nearest neighbour fermionic sites are horizontally or vertically connected on the lattice [Der+21]. We also need ancilla qubits labelled with a dashed index and shown in blue in figure 5. They are encoded as

$$h_{\text{hopping}}^{(i,j,\sigma)} \rightarrow \begin{cases} \frac{v}{2} (X_{i,\sigma} X_{j,\sigma} Y_{f_{ij}^{\uparrow},\sigma} + Y_{i,\sigma} Y_{j,\sigma} Y_{f_{ij}^{\downarrow},\sigma}) & \text{horizontal} \\ \frac{v}{2} (-1)^{g(i,j)} (X_{i,\sigma} X_{j,\sigma} X_{f_{ij}^{\uparrow},\sigma} + Y_{i,\sigma} Y_{j,\sigma} X_{f_{ij}^{\downarrow},\sigma}) & \text{vertical} \end{cases}. \quad (42)$$

In this notation i labels the data qubit for lattice site i and σ its spin lattice. Dashed indices such as f_{ij}^{\uparrow} refer to ancillary qubits for the fermionic encoding. The function $g(i,j)$ is either zero or one and depends on the details of the compact encoding [Der+21].

The locality of these Hamiltonian terms will increase when we introduce further ancilla qubits required to perform QEEP. These are shown in purple in figure 5. With planar connectivity this layout avoids the introduction of any SWAP gates, if one were only interested in one spin sector. To avoid SWAP overheads we therefore need a device with 3D connectivity. We must assume the device consists of two stacked and connected 2D grids of qubits with nearest neighbour connectivity, where one of these 2D grids is shown in figure 5.

To work out the individual costs of these now three and four local gates, we reference [CBC21, appendix B], and for an application of either term to time δ we obtain

$$\text{three-local on-site: } g_3(u, \delta) = g_3(u\delta) = \frac{|u\delta|}{2} + 2\sqrt{2|u\delta|} \quad (43)$$

$$\text{four-local hopping: } g_4(v, \delta) = g_4(v\delta) = 12\sqrt[3]{2|v\delta|} \quad (44)$$

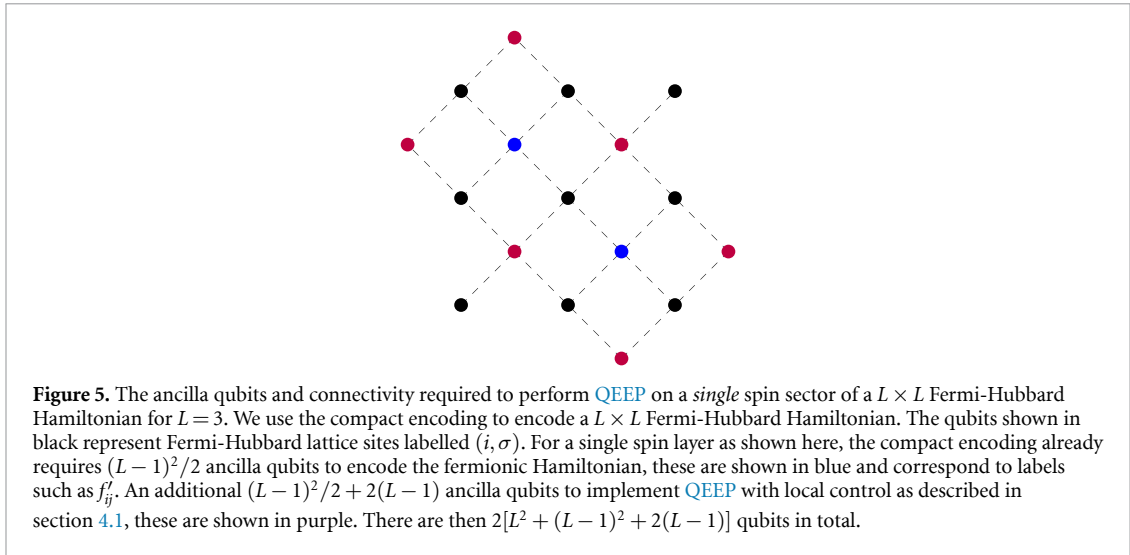
for a first order Trotter formula. We also remark that the compact encoding requires a single layer of the on-site terms, but four layers for the hopping terms; the total cost for a single Trotter step with time δ we have $g_3(u\delta) + 4g_4(v\delta)$. Additionally we assume the noise model explained in section 2.1 applies to this device and use equation (5) to calculate the run-time region where the combined stochastic and analytic error remains bounded by ϵ_{tar} for a variety of noise parameters q .

Now we will proceed to analyse QEEP and then rQEEP for a specific problem instance assuming this device connectivity. We will assume that our device has a given run-time budget before it is overcome by noise. We will determine numerically how the minimum obtainable bin-width η goes as a function of this run-time budget for various values of the target precision. That is we will perform the numerical equivalent of the asymptotic analysis of section 4.2 but solving equation (38) to get $\eta = \eta(\mathcal{T}, \epsilon)$.

In order to solve QEEP with a bin-width of η we must rescale H in order to apply the bound equation (73) or equation (69). For H on an $L \times L$ lattice, we know that $\|H\| \leq 5\Lambda$, where Λ is an upper bound on the norm of any of the groups of commuting interactions in the Trotter decomposition. We thus need to rescale the maximum evolution time by a factor $1/10\Lambda$. The maximum evolution time T is then bounded by

$$\text{Equation (73): } T \geq \frac{\pi}{10\eta\Lambda} \times \frac{e^{\pi\eta\epsilon/2}}{\sqrt{e^{\pi\eta\epsilon} - 1}}, \quad (45)$$

$$\text{Equation (69): } T \geq \frac{1}{5\eta\Lambda} \left(1 + \text{plog}_{-1} \left(-\frac{\epsilon\eta}{32e}\right)\right)^2, \quad (46)$$



where we are considering two possible choices of $f(\omega)$ with each choice leading to a different bound on the maximum evolution time as derived in appendix B. We assume $U'_c(T)$ is implemented by a p th-order Trotter formula using five layers. Each layer is made up of mutually commuting interactions which are also disjoint. We assume the NISQ device can implement these interactions in parallel (see [CBC21] for more details). The function $\eta = \eta(\mathcal{T}, \epsilon)$ has a further dependence on which order Trotter formula is used to implement $U'_c(T)$ as this determines \mathcal{T} . However in our numerical analysis we will simply show the minimum η obtained by varying over $p = 1, 2$ or 4. Furthermore we will use the numerical Trotter bounds obtained in [CBC21], based on extrapolating optimal Trotter step sizes from lattice sizes up to 3×3 .

To benchmark the impact of our sub-circuit synthesis techniques we perform the same analysis but restricting ourselves to decomposing the local unitaries into CNOT gates and single qubit rotations. We cost these gates in the same framework, meaning that in this case the run-time of each local Trotter step equals the circuit depth (disregarding single-qubit gates) of the decompositions of the three- and four-local interactions using the lowest-depth gate decomposition method (via conjugation), which yields

$$\text{three-local on-site: } g'_3(u, \delta) = g'_3 = \frac{5\pi}{4} \quad (47)$$

$$\text{four-local hopping: } g'_4(v, \delta) = g'_4 = \frac{5\pi}{2} \quad (48)$$

and again that a single layer has a runtime $g'_3 + 4g'_4$. The results of these numerics are presented in figure 1 and show that—within the parameter range considered—our asymptotically suboptimal choice of indicator function (solid lines) and synthesis techniques (red lines) yield improvements in the minimal achievable bin-width η for a given depolarizing noise rate and total runtime \mathcal{T} .

5. Discussion and conclusions

In this work we have investigated three different avenues of research concerning QPE. We recap and discuss them separately in the following.

5.1. Subcircuit analysis

We have built on our previous work, recapped in section 2, where we defined a non-standard circuit error model from an abstraction of the capabilities of NISQ hardware and then introduced gate synthesis techniques tailored to this framework. Here we have applied this framework to the problem of QEEP—introduced in [Som19]—to determine whether our gate synthesis techniques yield any improvements within this circuit error model.

In order to do this we have outlined a simple implementation of QEEP in section 4 aimed at minimizing runtime by performing controlled unitary evolution using only subcircuit gates. This QEEP implementation preserves any potential subcircuit gains, shown in [CBC21], by exchanging the global control ancilla of the QEEP implementation in [Som19] with local control ancillas and the creation of a global CAT state, in order to highlight its runtime minimizing properties within our minimize the runtime in the per-time error model. Note that we do not include the cost associated with measurement in our work, however this overhead will be a constant addition to both standard and subcircuit approaches.

It is essentially true by the definition of our per-time error model that our sub-circuit synthesis techniques will have an *asymptotic* advantage over standard synthesis techniques in this framework, as is shown in section 4.2. In addition to this, asymptotic analysis is of limited use within a NISQ context, as there may be large but hidden constants subsumed into big O notation. For both of these reasons we have anchored our conclusions in a *numerical* analysis of the 2D spin Fermi-Hubbard model. We have considered how implementing QEEP with local control relates to the connectivity of a NISQ device (see figure 5) and then perform numerics to obtain the results shown in figure 1. These plots demonstrate a numeric advantage for our synthesis techniques within a per-time error model. Modulo the applicability of a per-time error model, these techniques may allow one to perform a two bin instance of QEEP on an $L = 5$ spin Fermi-Hubbard model on hardware with a noise rate of $q = 10^{-5}$ while keeping the total error under 10%.

This encapsulates the first avenue of research explored in this paper, a development and application of our work in [CBC21] to assess the possibility of performing QEEP in the NISQ-era.

5.2. Reformulating QEEP

Secondly, we have reframed the QEEP protocol presented in [Som19] as an algorithm which allows one to sample from a convolution between the spectrum of a Hamiltonian, $G(\omega)$ and a freely chosen function $f(\omega)$ ¹¹. This is explained in section 2.3 and specifically via equation (16). By recasting the problem and algorithm in this way we hope to clarify which aspects we can modify and adapt to different computational problems.

Most trivially our analysis decouples the precision parameter ϵ from the bin-width η . However we have also explored the possibility of tailoring our choice of $f(\omega)$ to problem and parameter regime of interest, in our case an instance of QEEP with a Fermi-Hubbard Hamiltonian in a NISQ regime.

We define one such alternative indicator function in appendix B and compare the resultant lower bound on the maximum evolution time T with the original indicator function of [Som19] in figure 6. We emphasize that the original function gives asymptotically superior results, as it was intended to. Despite this, within the non-asymptotic parameter range of figure 1 we can see that for both standard and subcircuit synthesis techniques our bound gives improvements in the minimum obtainable η . For example, we estimate that the depolarizing single qubit error rate required to implement a minimum two bin example of QEEP—with a 5×5 Fermi-Hubbard model and up to a precision of $\epsilon = 0.1$ —can be reduced from 10^{-7} to 10^{-5} .

As we see from the above, the optimal choice of indicator function may depend on the task at hand. It is also possible that other applications might benefit from taking non-uniform samples from the time series $g(t)$ and employing more sophisticated classical signalling processing methods to reconstruct $p(\omega) = [G * f](\omega)$. By formulating QEEP as a protocol for sampling from a $p(\omega)$ we hope to make it easier to explore these questions in future work.

5.3. rQEEP

Finally, we suggest an application of QEEP having thus reformulated it as a general tool. We consider a problem analogous to matlab's `eig` or Mathematica's `Eigenvalues`. This was outlined in section 3.1 and in section 3.2 we demonstrate how to solve it using QEEP as a subroutine. We also incorporate this problem into our numerics as shown in figure 1 and find that it is more demanding than performing QEEP alone—as expected, due to the superior guarantees rQEEP gives on the placement of eigenvalues within each bin.

Data availability statement

No new data were created or analysed in this study.

Appendix A. Run-time of rQEEP

Here we prove theorem 5. We first note that if $y_i^{\text{hwr}} = y_i^{\text{upf}}$ for all i —which means that no eigenvalues were detected to lie in the shaded region shown for a single bin in section 3.2—the algorithm would return an answer to the rQEEP. The issue is that we cannot be certain that H has no eigenvalues in these regions; and furthermore, since the q_i are *approximate* (since they include Fourier truncation and measurement errors) it is unlikely that any of them will be precisely zero.

However, we can estimate with what likelihood any of H 's eigenvalues lie these regions. As these ambiguous shaded regions are centred around the x_i 's, we can derive an expected number of eigenvalues that will lie within the ambiguous region. We use the following lemma:

¹¹ Freely chosen from functions which satisfy the conditions explained in section 2.3.

Lemma 4. *let the setup be as in the rQEEP algorithm outlined in section 3 but given an ideal QEEP solver with $\epsilon = 0$ or equivalently $\mathbf{p} = \mathbf{q}$. Then*

$$\mathbb{E} \left[\sum_i (y_i^{\text{upr}} - y_i^{\text{lwr}}) \right] \leq 2^Q \times 6\eta(m+1)^2. \tag{49}$$

Proof. It is easy to see that any ambiguous region between the two envelopes R_i^{lwr} and R_{i+1}^{lwr} has width 2η , and hence leaves room for up to two bin centres w_j , let us call them w_a and w_b . Neither of the q_a, q_b will be counted in $y_i^{\text{lwr}}, y_{i+1}^{\text{lwr}}$, but both will be counted in $y_i^{\text{upr}}, y_{i+1}^{\text{upr}}$. This means that the ambiguous region around w_a, w_b has width 3η (left support end of $f(w_a)$ till right support end of $f(w_b)$). Noting that overlapping ambiguous regions (e.g. when x_i and x_{i+1} are very close) just reduce the overall ambiguous area, the remainder of the proof is a volume argument: if we consider a *fixed* index i and look at the ambiguous regions to the right (associated with x_i) and the left (associated with x_{i-1}), the position of right region is chosen uniformly at random from S_i and position of left region is chosen uniformly at random from S_{i-1} . For each eigenvalue and ambiguous region we can define a function, $\chi_{i,\lambda}(x_i) \in \{1, 0\}$, which indicates whether the ambiguous region associated with x_i contains the eigenvalue λ . Now we consider the random variables $\chi_\lambda(x_i)$ and $\chi_\lambda(x_{i-1})$ where we have made the i subscript implicit through the variable x_i . As each ambiguous region is chosen from a segment of width $\xi/2$ the probability that $\chi_\lambda(x_i) = 1$ is upper bounded by $6\eta/\xi$ and likewise for $\chi_\lambda(x_{i-1})$. As expectation values are linear even for correlated random variables we can say that

$$\mathbb{E}[\chi_\lambda(x_{i-1})] + \mathbb{E}[\chi_\lambda(x_i)] = \mathbb{E}[\chi_\lambda(x_{i-1}) + \chi_\lambda(x_i)] \leq \frac{12\eta}{\xi}, \tag{50}$$

and by the same argument that

$$\mathbb{E} [n_i^{\text{upr}} - n_i^{\text{lwr}}] = \mathbb{E} \left[\sum_\lambda (\chi_\lambda(x_{i-1}) + \chi_\lambda(x_i)) \right] \leq 2^Q \times \frac{12\eta}{\xi}. \tag{51}$$

Jointly, the position of the ambiguous intervals is of course not uncorrelated, since we choose each within a constrained segment; but again we use the fact that expectation values are linear, and so we have

$$\sum_{i=1}^{m+1} \mathbb{E} [y_i^{\text{upr}} - y_i^{\text{lwr}}] = \mathbb{E} \left[\sum_{i=1}^{m+1} (y_i^{\text{upr}} - y_i^{\text{lwr}}) \right] \leq 2^Q \times 6\eta(m+1)^2. \tag{52}$$

The claim follows. □

Theorem 5. *If assume access to a QEEP solver with quantum runtime $\mathcal{T}(Q, \eta, \epsilon, c)$ then the following holds. For a point spacing $\xi > 0$ (or equivalently $m := 2/\xi$), deviation $\Delta \geq 0$, and confidence c , the overall quantum runtime to answer rQEEP using rQEEP is*

$$\mathcal{T} \left(Q, \frac{1}{12(m+1)^2} \times \frac{\Delta}{2^Q}, \frac{1}{16} \times \frac{\Delta}{2^Q}, c \right), \tag{53}$$

and the additional classical overhead is $\log_{(1-\frac{\xi}{2})}(1-c)$.

Proof. To prove that the algorithm does indeed answer rQEEP is now straightforward: in every run of the subloop, QEEP succeeds with probability c to produce the desired probability vector q which satisfies $|\mathbf{p} - \mathbf{q}| \leq \epsilon$. Then if y'_i is constructed from elements of \mathbf{p} and y_i denotes the actual output of the algorithm and is constructed from elements of \mathbf{q} we have

$$\sum_i |y_i - n_i| \leq \sum_i |y_i - y'_i| + \sum_i |y'_i - n_i|. \tag{54}$$

We first consider the second term. The envelope method for the chosen bin width produces an estimate y'_i of $n_i \in [y_i^{\text{lwr}}, y_i^{\text{upr}}]$. Then using Markov's inequality and lemma 4 we can say that with probability $\geq 1/2$ and that

$$\sum_i (y_i^{\text{upr}} - y_i^{\text{lwr}}) < 2 \times \mathbb{E} \left[\sum_i (y_i^{\text{upr}} - y_i^{\text{lwr}}) \right], \tag{55}$$

and therefore that with probability $\geq 1/2$ that

$$\sum_i |y'_i - n_i| = \sum_i \left| \frac{y_i^{\text{upr}} + y_i^{\text{lwr}}}{2} - n_i \right| \quad (56)$$

$$\leq \frac{1}{2} \sum_i |y_i^{\text{upr}} - y_i^{\text{lwr}}| \quad (57)$$

$$\leq 2^Q \times 6(m+1)^2 \times \frac{\Delta}{2^{Q+1}6(m+1)^2} = \frac{\Delta}{2}. \quad (58)$$

We now consider the first term. From Somma's analysis we have that $\forall j |q_j - p_j| \leq \epsilon/(M+1)$, and by definition $M = \lfloor 1/\eta \rfloor$ so we have

$$\sum_{i=1}^{m+1} |y_i - y'_i| \leq 2^Q \sum_i \sum_{\omega_j \in R_i^{\text{upr}}} |q_j - p_j| \quad (59)$$

$$\leq 2^Q \sum_{i,\omega_j} \frac{\epsilon}{M+1} \leq 2^Q \sum_{i,\omega_j} \frac{\epsilon}{M}. \quad (60)$$

By definition $|x_i - x_{i-1}| \leq \xi$. The width of R_i^{upr} is then at most $\xi + 2\eta$. If we assume that $\xi/\eta > 2$ then there are at most $(\xi + 2\eta)/\eta \leq 2\xi/\eta$ bins labelled by ω_j in R_i^{upr} and therefore

$$\sum_{i=1}^{m+1} |y_i - y'_i| \leq 2^Q \sum_i \left(\frac{2\xi}{\eta} \times \frac{\epsilon}{M} \right) = 2^{Q+1} \sum_i \xi \epsilon. \quad (61)$$

As $\xi = 2/m$ and $m+1 < 2m$ this simplifies to

$$\sum_{i=1}^{m+1} |y_i - y'_i| \leq 2^{Q+1} \times 2m \times \xi \epsilon \quad (62)$$

$$= 4 \times 2^{Q+1} \epsilon = \frac{\Delta}{2}. \quad (63)$$

If this bound succeeded, the overall deviation due to the envelope, plus the QEEP deviation due to the precision parameter $\epsilon = \Delta/(8 \times 2^{Q+1})$, thus leads to a deviation $\sum_j |y_j - n_j| \leq \Delta$.

In order to ensure that the overall procedure succeeds with confidence at least c , we note that the success probability of one run of the subloop is now $c/2$ (the c from QEEP, the $1/2$ from the deviation in expectation of the envelope method). From the opposite perspective, the likelihood of failure of all rounds is thus

$$\left(1 - \frac{c}{2}\right)^{\lceil \log_{(1-\frac{c}{2})}(1-c) \rceil} \leq 1 - c, \quad (64)$$

and hence the overall success probability is lower-bounded by the desired confidence level c . The theorem statement then follows. \square

Appendix B. QEEP indicator functions

B.1. Alternative indicator function

Computing an explicit lower bound for T using Somma's original indicator function is a non-trivial task. We include an asymptotic calculation in appendix B.2. However for near term applications, a simpler indicator function may yield better analytic bounds in the non-asymptotic regime. For this reason we consider a different indicator function, which allows us to derive an explicit bound on T without further restrictions when said bound holds. To this end—and re-using the symbols f_j and F_j in the following—we define

$$f(w) := \begin{cases} \cos^2\left(\frac{\pi w}{2\eta}\right) & -\eta < w < \eta \\ 0 & \text{otherwise.} \end{cases} \quad (65)$$

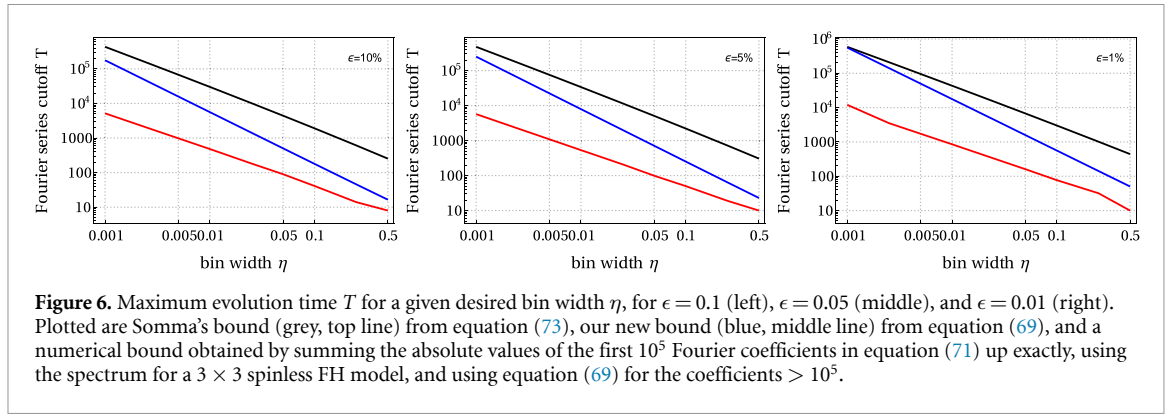


Figure 6. Maximum evolution time T for a given desired bin width η , for $\epsilon = 0.1$ (left), $\epsilon = 0.05$ (middle), and $\epsilon = 0.01$ (right). Plotted are Somma's bound (grey, top line) from equation (73), our new bound (blue, middle line) from equation (69), and a numerical bound obtained by summing the absolute values of the first 10^5 Fourier coefficients in equation (71) up exactly, using the spectrum for a 3×3 spinless FH model, and using equation (69) for the coefficients $> 10^5$.

It is easy to check that these indicator functions satisfy the conditions of QEEP. Furthermore, we can explicitly derive its Fourier transform (and thus the Fourier series coefficients) from equation (20), namely

$$F(t) = \begin{cases} \frac{\pi \sin(t\eta)}{2t\pi^2 - 2t^3\eta^2} & t \neq 0 \\ \frac{\eta}{2\pi} & \text{otherwise} \end{cases} \quad (66)$$

and thus for $t > \pi/\eta$ we have

$$|F(t)| \leq \frac{1}{2\pi} \times \frac{1}{t^3\eta^2/\pi^2 - t}. \quad (67)$$

Together with equation (24) we then get

$$|p_j - p'_j| \leq \frac{1}{2\pi} \sum_{|t|>T} \frac{\pi^2}{t^3\eta^2 - t\pi^2} \leq \frac{1}{2\pi} \int_T^\infty \frac{\pi^2}{t^3\eta^2 - t\pi^2} dk = \frac{1}{4\pi} \log \left(\frac{\eta^2 T^2}{\eta^2 T^2 - \pi^2} \right) \stackrel{!}{\leq} \frac{\epsilon}{2(M+1)} \quad (68)$$

which together with $M + 1 \leq 2/\eta$ yields

$$T \geq \frac{\pi}{\eta} \times \frac{e^{\pi\eta\epsilon/2}}{\sqrt{e^{\pi\eta\epsilon} - 1}}. \quad (69)$$

Both for equations (69) and (73) we gain a factor of M in case we are interested in the max-norm instead of the one-norm, as mentioned. We compare this new bound with Somma's bound in figure 6.

B.2. Original indicator function

In this section we find a lower bound on the Fourier series cutoff T in equation (24), when using Somma's indicator function, as described in section 2.3. We wish to determine the minimal T such that

$$\|\mathbf{p} - \mathbf{p}'\| \leq \frac{\epsilon}{2}, \quad (70)$$

where \mathbf{p} is given in equation (22). By equations (24) and (22), we have

$$|p_j - p'_j| \leq \sum_{|t|>T} |F_t^j| |g_t|. \quad (71)$$

Since $|g_t| \leq 1$, it suffices to find a bound F_t^j . Assuming that T is chosen large enough such that equation (23) holds gives us

$$|p_j - p'_j| \leq \sum_{|t|>T} \eta \left| \exp \left(-\sqrt{|t|\eta/2} \right) \right| \leq 2\eta \int_{t=T}^\infty \exp \left(-\sqrt{|T|\eta/2} \right) dt = 8e^{-\sqrt{T\eta/2}} \left(1 + \sqrt{T\eta/2} \right). \quad (72)$$

Distributing $\epsilon/2$ equally amongst the $M + 1 \leq 2M$ bins gives the bound on the Fourier truncation T for $T \geq \alpha/\eta$

$$e^{-\sqrt{T\eta/2}} \left(1 + \sqrt{T\eta/2} \right) \stackrel{!}{\leq} \frac{\epsilon}{32M} \implies T \geq \frac{2}{\eta} \left(1 + \text{plog}_{-1} \left(-\frac{\epsilon\eta}{32e} \right) \right)^2. \quad (73)$$

Here the product logarithm $\text{plog}_{-1}(y)$ denotes the -1 th solution for w in the equation $y = we^w$, this is also known as the Lambert W function. We emphasise that this is an asymptotic result, finding α is not straightforward.

ORCID iD

Laura Clinton  <https://orcid.org/0000-0002-4102-4741>

References

- [AA17] Atia Y and Aharonov D 2017 Fast-forwarding of Hamiltonians and exponentially precise measurements *Nat. Commun.* **8** 1–9
- [BFS11] Brown B, Flammia S T and Schuch N 2011 Computational difficulty of computing the density of states *Phys. Rev. Lett.* **107** 040501
- [CBC21] Clinton L, Bausch J and Cubitt T 2021 Hamiltonian simulation algorithms for near-term quantum hardware *Nat. Commun.* **12** 1–10
- [Der+21] Derby C, Klassen J, Bausch J and Cubitt T 2021 Compact fermion to qubit mappings *Phys. Rev. B* **104** 035118
- [HMH05] Hartmann M, Mahler G and Hess O 2005 Spectral densities and partition functions of modular quantum systems as derived from a central limit theorem *J. Stat. Phys.* **119** 1139–51
- [HMH04] Hartmann M, mahler G and Hess O 2004 Gaussian quantum fluctuations in interacting many particle systems *Lett. Math. Phys.* **68** 103–12
- [IFT98] Imada M, Fujimori A and Tokura Y 1998 Metal-insulator transitions *Rev. Mod. Phys.* **70** 1039–263
- [Kit95] Kitaev A Y 1995 Quantum measurements and the Abelian stabilizer problem (arXiv:quant-ph/9511026)
- [Kit04] Kittel C 2004 *Introduction to Solid State Physics* 8th edn (New York: Wiley)
- [LT21] Lin L and Tong Y 2021 Heisenberg-limited ground state energy estimation for early fault-tolerant quantum computers (arXiv:2102.11340)
- [OTT19] O’Brien T, Tarasinski B and Terhal B 2019 Quantum phase estimation of multiple eigenvalues for small-scale (noisy) experiments *New J. Phys.* **21** 023022
- [Sho97] Shor P W 1997 Polynomial-time algorithms for prime factorization and discrete logarithms on a quantum computer *SIAM J. Comput.* **26** 1484–509
- [Som19] Somma R 2019 Quantum eigenvalue estimation via time series analysis *New J. Phys.* **21** 123025
- [Ste+21] Stenger J P T, Bronn N T, Egger D J and Pekker D 2021 Simulating the dynamics of braiding of majorana zero modes using an IBM quantum computer *Phys. Rev. Res.* **3** 033171
- [WZ06] Wocjan P and Zhang S 2006 Several natural BQP-complete problems (arXiv:quant-ph/0606179)